INVESTIGATION OF OLIVE STONES PYROLYSIS *VIA* COUPLED THERMOGRAVIMETRIC ANALYSIS-MASS SPECTROMETRY: THERMAL BEHAVIOR AND KINETIC PARAMETERS

AMINA BEDOUI,[*] SOUAD SOUISSI-NAJAR,[*] SITI SHAWALLIAH IDRIS,[**] NORAZAH ABD RAHMAN[**] and ABDELMOTTALEB OUEDERNI[*]

[*]*Laboratory of Process Engineering and Industrial Systems (LR11ES54), National School of Engineers of Gabes, University of Gabes, St Omar Ibn El Khattab, 6029, Gabes, Tunisia*
[**]*Department of Chemical Engineering, College of Engineering, Universiti Teknologi MARA Malaysia, 40450 Shah Alam, Selangor, Malaysia*
✉ *Corresponding author: A. Bedoui, amina.bedoui@gmail.com*

Received December 11, 2021

The pyrolysis of olive stones was investigated by thermogravimetric analysis-mass spectrometry in nitrogen atmosphere under non-isothermal conditions, at heating rates of 5, 10, 20, and 30 °C/min. According to gas evolution analysis, the thermal degradation of olive stones under inert atmosphere can be divided into four stages. There was only dehydration in the first stage (<200 °C). Most of gas products (CO_2, CO, CH_4, C_2H_6 and H_2O) were evolved in the second stage in the temperature range 210-407 °C, simultaneously with main mass degradation. Only H_2 was produced in the fourth stage at high temperatures (>550 °C). Thermogravimetric analysis results have been utilized to determine kinetic parameters by using a composite procedure involving the iso-conversional method (Flynn-Wall-Ozawa and Kissinger-Akahira-Sunose) and the master-plots method. The activation energy values estimated by the Ozawa-Flynn-Wall and the Kissinger-Akahira-Sunose methods are very close, with values of 229.20 kJ/mol and 232.55 kJ/mol, respectively. The master-plots method shows that the most probable reaction mechanism was described by an order n (O_n) model. The frequency factor was estimated to be $A = 5.6 \times 10^{21}$ min^{-1}, the kinetic exponent was n = 6.2, and the reaction model function was $f(\alpha) = (1-\alpha)^{6.2}$.

Keywords: olive stones, pyrolysis, kinetic, TGA-MS, master-plots method

INTRODUCTION

Olive oil production is of a great economical importance in many Mediterranean countries, *i.e.* Spain, Italy, Turkey, Greece, and Tunisia. These countries are the largest olive oil producers in the world as they marketed 97% of the world olive oil production.[1,2] Tunisia is among the largest exporters of olive oil worldwide. It is considered as one of the most experienced countries with regards to the cultivation of olive trees in the southern Mediterranean region; over 30% of its arable land is devoted to olive cultivation.

It is a well-known fact that the production of olive oil generates large volumes of wastes. These big quantities of bio-waste, especially olive stones, become an environmental problem to the oil producing country. Several researches have proved that energetic valorization is a solution for solid waste elimination.[3-5] Therefore, using biomass to produce bioenergy is often a way to dispose of waste materials that otherwise would create environmental risks. The exploitation of biomass for producing energy is an interesting challenge since it is net zero CO_2 emission, abundantly available and minimizes the disposal problems associated with the generation of agricultural by-products. Thermo-chemical conversion methods, including combustion, gasification and pyrolysis, are the most common ones to upgrade biomass energy quality.[5-7] It has been widely reported that using agricultural by-products as a renewable source of energy by means of pyrolysis processes, is absolutely feasible.[5,6,8,9] Pyrolysis is one of the most often employed methods to convert biomass and organic residues into various products. Solid biomass and organic wastes, which are difficult

and costly to manage, can be readily converted into liquid, gas and charcoal products through the pyrolysis process. Therefore, research on the pyrolysis process of a specific lignocellulosic waste would be beneficial for a better understanding of the pyrolytic mechanism and to improve its transformation into and application as bio-fuels, chemical products and bio-materials. So, among the many reasons for quantifying the rate of a chemical reaction, the thermo-kinetic behavior of the biomass is of high importance during the degradation of its main components. This behavior allows us to control the reaction rate as a function of temperature and composition.

Thermal analysis has proved to be a powerful tool for investigating the pyrolysis of biomass. Numerous studies based on thermogravimetric analysis (TGA) and derivative thermogravimetry (DTG) have been carried out.[4,5,10,11] However, TGA/DTG might not seem sufficient for a thorough study based on kinetics. Therefore, other techniques must be used to obtain valuable results. TGA coupled with mass spectrometry (MS) provides the conditions for real-time (online) quantitative and qualitative evolved gas analysis. The utilization of the MS techniques, along with thermal analysis, can facilitate a deeper insight into the kinetic scheme and, consequently, to understand the actual reaction mechanism. Although there has been quite a lot of research about the pyrolysis of olive stones as a lignocellulosic biomass, such as kinetics and product analysis[4,8,10,12] detailed studies on the distribution of specific products with reaction temperature and time are relatively few.[13,14] To our knowledge, there is no paper studying Tunisian olive stones pyrolysis via TGA-MS.

TGA results can be used for kinetic analysis of thermolysis processes. A kinetic model is necessary to predict the thermolysis behavior, to design the necessary equipment and to determine their operation conditions. Kinetic parameters can be evaluated using model-fitting or model-free techniques. When the reaction mechanism of thermal decomposition cannot be predetermined, model-free methods offer a simple and powerful tool to estimate activation energy by using data from a series of experiments at different heating rates.[5,15] The model-free approach does not require assumption of specific reaction models, and yields unique kinetic parameters as a function of either conversion or temperature. According to this model, a single step process is considered and the need for an accurate reaction scheme is eliminated. Most recent researchers have used free methods in order to determine the kinetics of different kinds of biomass, such as palm stems, cashew nut shells, bagasse, coffee husks,[16] pinyon pine,[11] and micro-algae.[15,16] Thus, the present study aimed to investigate the thermogravimetric property, pyrolysis kinetics and gas product distribution of olive stones pyrolysis by using the TGA–MS technology. The thermal degradation characteristics were studied under inert conditions at different heating rates of 5, 10, 20, and 30 °C/min. The kinetic parameters of thermal decomposition were obtained by iso-conversional Ozawa-Flynn-Wall (OFW) and Kissinger-Akahira-Sunose (KAS) models, and the thermal reaction mechanism of olive stones was estimated by using the master-plots method.

EXPERIMENTAL

Materials

Olive stones (OS) are a by-product resulting from Tunisian oleic manufacture. The precursor was washed several times with distilled water, air dried until constant humidity, prior to any analysis. The obtained sample was ground in a mill (model number OCT-609709) and sieved with a sieve model Endecotts Octagon 2000 to yield powder samples (<400 µm). The samples prepared were referred to as OS (olive stone). In the present study, no chemical treatment was undertaken.

Characterization of initial samples

Proximate analysis of the samples was performed based on ASTM methods E871, E872-82 and D1102-84 using a TGA/SDTA851^e thermobalance manufactured by Mettler Toledo.

Approximately 20 mg of the sample was loaded into a 150 µL aluminium ceramic crucible. The sample was heated continuously from room temperature to 950 °C in nitrogen atmosphere. At this temperature, oxygen was injected to oxidize the residual carbon formed during the pyrolysis step and thus, to identify the ash content, keeping the same nitrogen flow rate (50 mL/min) up to a temperature of 1100 °C. The determination of each component was done by integration using the software predefined by Mettler Toledo.

Meanwhile, elemental analysis was performed in a CHNS-O analyzer (model Thermo FinneganFlashea 1112) according to ASTM D 5373-02. The oxygen content of the sample was obtained from mass balance among C, H, S and N. The calorific value was determined based on ASTM D 2015-96 *via* an Ika Works C5000 calorimeter.

Thermal analysis (TGA)

The pyrolysis of OS was firstly carried out in a TGA apparatus (TGA-DSC 1, METTLER TOLEDO). An approximate weight of 20 mg of the initial sample, with a particle size lower than 400 µm, was loaded into a 150 µL ceramic alumina crucible under non-isothermal conditions. The sample was heated from 30 to 750 °C at different heating rates (5, 10, 20 and 30 °C/min). Nitrogen was used as carrier gas, to provide an inert atmosphere with a flow rate of 50 mL.min^{-1}.

Thermoanalytical measurements TGA-MS analysis

TGA (Mettler-Toledo TGA/SDTA 851^{e}) coupled with mass spectrometer (Pfeiffer Vacuum-Thermostar^{TM}) was utilized to analyze the OS thermal behavior and detect the released gases simultaneously. Approximately 20 mg of sample was loaded into an alumina crucible pan and heated from room temperature to 750 °C at a heating rate of 10 °C.min^{-1}. All experiments used pure nitrogen (99.999%) as carrier gas. In order to identify ions with m/z in the range 0-300, a preliminary broad scan was performed at a heating rate of 10 °C.min^{-1}. The signals identified corresponded to the mass spectra of 2, 16, 18, 28, 30 and 44 a.m.u, which correspond to the main components of the pyrolysis gas (H_2, CH_4, H_2O, CO, C_2H_6 and CO_2, respectively).

Kinetic modeling

The solid-state pyrolysis kinetics of biomass using different models has been investigated by several researchers.[5,6] The rate of reaction for the decomposition of a solid depends on the temperature and the amount of substance. Thus, the common rate equation for the kinetic analysis can be generally expressed as follows:

$$\frac{d\alpha}{dt} = k(T)f(\alpha) \quad (1)$$

where α is the conversion degree, t is time, T is the absolute temperature, k (T) is the temperature dependent rate constant, f(α) is a function relating to the reaction mechanism, α is expressed as:

$$\alpha = \frac{m_0 - m}{m_0 - m_\infty} \quad (2)$$

where m_0, m and m_∞ refer to initial, instantaneous and final sample mass, respectively.

According to the Arrhenius equation, k(T) is usually expressed as follows:

$$k(T) = A\exp(-\frac{E_a}{RT}) \quad (3)$$

where A is the pre-exponential factor (min^{-1}), E_a is the activation energy of the reaction (J/mol), R is the universal gas constant (8.314 J/mol K), and T is the absolute temperature (K). By substituting Equation (3) in Equation (1), gives:

$$\frac{d\alpha}{dt} = A\exp(-\frac{E_a}{RT})f(\alpha) \quad (4)$$

Taking into account that the temperature is time variable and it increases linearly with a constant heating rate, β, the following expression is derived:

$$T = \beta t + T_0 \quad (5)$$

$$dT = \beta dt \quad (6)$$

Combining Equations (4) and (6), and rearranging them gives:

$$\frac{d\alpha}{dT} = \frac{A}{\beta}\exp(-\frac{E_a}{RT})f(\alpha) \quad (7)$$

Integrating Equation (7), we get:

$$g(\alpha) = \int_0^\alpha \frac{d\alpha}{f(\alpha)} = \int_0^T \frac{A}{\beta}\exp(-\frac{E_a}{RT})dT = \frac{AE_a}{\beta R}\int_u^\infty u^{-2}e^{-u}du = \frac{AE_a}{\beta R}P(u) \quad (8)$$

where g(α) is the integrated form of the conversion dependence function f(α). The temperature integral $\int_u^\infty u^{-2}e^{-u}du$ (u = E_a/RT) has no analytical solution and can be expressed by an approximation. The rational approximation of Doyle[17] gives sufficiently accurate results. Thus, Equation (8) can be solved by numerical methods or approximations. Based on these equations, different kinetic methods were applied in this study.

Iso-conversional models

It is well known that the iso-conversional method easily gives an estimate of activation energy, without prior knowledge of the reaction mechanism. These methods are model-free and evaluate the activation energy at progressive values of conversion. These assumed that the reaction kinetics is independent of the heating rate and the conversion of raw materials occurs in a simple one-step process.[5] Two kinds of iso-conversional methods are applied in this paper: Ozawa-Flynn-Wall (OFW) and Kissinger–Akahira-Sunose (KAS) models.[18,19]

OFW model

The Ozawa-Flynn-Wall (OFW) method is based on Doyle's approximation, where u = E/RT:[5]

$$P(u) = 0.00484 + \exp(-1.0516u) \quad (9)$$

By substituting Doyle's approximation into Equation (8) and expressing in logarithmic form, we obtain:

$$\ln(g(\alpha)) = \ln(\frac{AE_a}{\beta R}) + \ln(P(u)) \quad (10)$$

$$\ln(\beta) = \ln\left[\frac{AE_a}{Rg(\alpha)}\right] - 5.34 - 1.516\frac{E_a}{RT} \quad (11)$$

When α = constant, the values of ln β versus 1/T, obtained at several β, could be correlated by a straight line of which the slope allows E_a determination.

KAS model

The Kissenger-Akahira-Sunose (KAS) method[18] introduces an approximation of:

$$P(u) = u^{-2}e^{-u} \quad (12)$$

into Equation (8), and after rearrangement, the expression becomes:

$$g(\alpha) = \frac{AE_a}{\beta R} u^{-2} e^{-u} \quad (13)$$

Expressing Equation (13) in logarithmic form:

$$\ln(g(\alpha)) = \ln(\frac{T^2}{\beta}) + \ln(\frac{AR}{E_a}) - \frac{E_a}{RT} \quad (14)$$

$$\ln(\frac{\beta}{T^2}) = \left[\ln(\frac{AE_a}{Rg(\alpha)}) \right] - \frac{E_a}{RT} \quad (15)$$

E_a can be determined from the slope of the line generated through a linear correlation $\ln(\frac{\beta}{T^2})$ vs 1/T, as well.

Master-plots method

The reaction models of decomposition reactions can be determined by using the master-plots method. Taking into account a single-step process, the kinetic model, A and E_a are invariable.[15] Using a reference at point $\alpha = 0.5$ and according to Equation (8), we can get the equation as follows:

$$g(0.5) = \frac{AE_a}{\beta R} P(u_{0.5}) \quad (16)$$

where g (0.5) is the value of the selected g (α) function at conversion $\alpha = 0.5$ and $u_{0.5} = \langle E_a R/T \rangle_{0.5}$ is the value of u at conversion $\alpha = 0.5$. The following equation is obtained by dividing Equation (8) by Equation (16):

$$\frac{g(\alpha)}{g(0.5)} = \frac{P(u)}{P(u_{0.5})} \quad (17)$$

$$P(u) = 0.00484 + \exp(-1.0516\, u) \quad (18)$$

The theoretical master plots of various g(α) functions was generated by plotting g(α)/g(0.5) against α. Table 1 shows the most frequently used mechanism for the solid state process and the reaction model (f (α), g (α)). The experimental master plots of P(u)/ $P(u_{0.5})$ against α may be obtained from experimental data under any heating rate. Equation (17) indicates that, for a given α, the experimental value of P (u)/P $(u_{0.5})$ and the theoretically calculated value of g(α)/g(0.5) are equivalent for a given conversion α when an appropriate reaction model is selected.[15,20] This integral master-plots method can be used to determine the reaction kinetic models of decomposition reactions.

RESULTS AND DISCUSSION

Proximate and ultimate analyses

Table 2 depicts the results of OS proximate and ultimate analyses and chemical composition. The volatile matter and the fixed carbon content of OS were 67.88 and 21.64 wt%, respectively. The moisture and ash contents of OS were 10.24 and 0.24 wt%, respectively. Furthermore, the low ash content in OS minimized the effect of catalytic behavior of the mineral contents to produce non-condensable gases and it led to the bio-oil yield improvement during pyrolysis.

Table 1
Most frequently used mechanisms of solid-state processes

Mechanism	Symbol	f(α)	$g(\alpha) = \int_0^\alpha \frac{d\alpha}{f(\alpha)}$
Order of reaction			
First order	O1	$(1-\alpha)$	$-\ln(1-\alpha)$
Second order	O2	$(1-\alpha)^2$	$(1-\alpha)^{-1}-1$
Third order	O3	$(1-\alpha)^3$	$(1-\alpha)^{-2}-1$
Diffusion			
One-way transport	D1	$1/(2\alpha)$	α^2
Two-way transport	D2	$[-\ln(1-\alpha)]^{-1}$	$(1-\alpha)\ln(1-\alpha)+\alpha$
Three-way transport	D3	$3/2(1-\alpha)^{2/3}[1-(1-\alpha)^{1/3}]^{-1}$	$[1-(1-\alpha)]^{1/3}]^2$
Ginstling-Brounshtein equation	D4	$3/2[(1-\alpha)^{1/3}-1]^{-1}$	$(1-2\alpha/3)-(1-\alpha)^{2/3}$
Limiting surface reaction between both phases			
One dimensional	R1	1	α
Two dimensional	R2	$2(1-\alpha)^{1/2}$	$1-(1-\alpha)^{1/2}$
Three dimensional	R3	$3(1-\alpha)^{2/3}$	$1-(1-\alpha)^{1/3}$
Random nucleation and nuclei growth			
Two dimensional	A2	$3(1-\alpha)[-\ln(1-\alpha)]^{2/3}$	$[-\ln(1-\alpha)]^{1/3}$
Three dimensional	A3	$4(1-\alpha)[-\ln(1-\alpha)]^{3/4}$	$[-\ln(1-\alpha)]^{1/4}$
Exponential nucleation			
Power law, n = 1/2	P2	$2\alpha^{1/2}$	$\alpha^{1/2}$
Power law, n = 1/3	P3	$3\alpha^{2/3}$	$\alpha^{1/3}$
Power law, n = 1/4	P4	$4\alpha^{3/4}$	$\alpha^{1/4}$

The moisture content plays an important role in the selection of the biomass conversion route. Biomass with higher moisture content is preferred for biochemical conversion, while biomass with lower moisture content is favorable for the thermo-chemical conversion process. Low moisture content makes the OS to be suitable for a thermal conversion process like pyrolysis.

Table 2
Sample characteristics of OS

Proximate analysis (wet basis %)	
Fixed carbon	21.64
Volatile matter	67.88
Moisture	10.24
Ash	0.240
Ultimate analysis (wet basis %)	
C	35.81
H	4.55
N	0.67
S	< 0.20
O*	58.77
H/C	1.52
O/C	1.23
Empirical formula	$CH_{1.52}O_{1.23}N_{0.016}$
Chemical composition (wet basis %)	
Cellulose	38.25
Hemicelluloses	16.77
Lignin	40.00
Extractives	2.50
HHV (kJ/kg)	18.86

*By difference

Table 2 also shows the ultimate analysis of olive stones. The results show that OS is a C (35.81 wt%) and O (58.77 wt%) rich raw biomass material, also containing 4.55% of H and trace amounts of N (0.67 wt%). Nevertheless, the S content presents a low value (<0.20%). The low content of nitrogen and sulfur is interesting with respect to the application of OS in gasification and pyrolysis processes. In addition, the O/C and H/C atomic ratios were mentioned. The O/C and H/C ratio ranges were 1.23 and 1.52, respectively. The empirical formula of OS is $CH_{1.52}O_{1.23}N_{0.016}$. Olive stones consist of cellulose, hemicelluloses and lignin, in addition to extractives, water and mineral matter. The high lignin contents (40% of total solids) versus 55% of holocellulose contents of olive stones can be clearly remarked.

Chemical structure evaluation

The FTIR spectrum of raw OS is shown in Figure 1. The FTIR signals with their assignments and the typical functional groups are listed in Table 3. It is clear that the infrared spectrum of olive stones is similarly shaped to the spectra recorded for other lignocellulosic materials in the literature.[21,22]

The band located at 3344 cm^{-1} corresponds to the O–H stretching vibrations in hydroxyl, acid and phenol groups, being indicative of the lignin polymer.[23] Meanwhile, the band located at 2882 cm^{-1} is due to the C–H stretching vibrations of CH, CH_2 and CH_3 groups in methyl and methylene groups. These two bands indicate, respectively, the lignin and hemicelluloses polymers.[23]

The band at 1724 cm^{-1} is ascribed to the carbonyl C=O groups.[24] Olefinic (C=C) vibrations caused the emergence of the band at about 1651 cm^{-1}, while the skeletal C=C vibrations in aromatic rings caused another two bands to emerge at 1594 and 1511 cm^{-1}.[25] The vibrations at 1428 and 1363 cm^{-1} are assigned to the bands of C-H and O-H, forming a basic structure of this lignocellulosic biomass.[21] The band at 1311 cm^{-1} and at 1229 cm^{-1} can be attributed to (C–O) vibrations in carboxylate groups and to esters (*e.g.* R–CO–O–R_), ethers (*e.g.* R–O–R_) or phenol groups, respectively.[22] The relatively intense band at 1029 cm^{-1} can be assigned to C-O, C=C and C-C-O stretching, corresponding to cellulose, hemicelluloses and lignin polymers.[23]

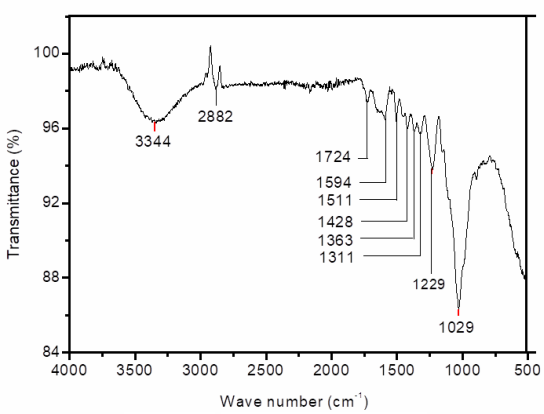

Figure 1: FT-IR spectra of OS

Table 3
Assignment of peaks to the chemical functional groups and biomass components via FTIR for raw OS

Wavenumber (cm^{-1})	Vibration	Functional groups	Biomass component	Ref.
3700-3000	O-H (stretching)	Phenolic, alcoholic, carboxylic	Lignin	[23]
3000-2800	C-H (stretching)	$-CH_2$, $-CH_3$	Lignin, hemicellulose	[23]
1730	C=O (stretching)	Carbonyl	Hemicelluloses	[24]
1650-1500	C=C (stretching)	Aromatic structure	Lignin	[22]
1700-1600	C=C (stretching)	Olefin structure	Lignin	[22]
1430-1360	O-H, C-H	Alcoholic, carboxylic, phenol, olefinic	Lignin, cellulose, Hemicelluloses	[22, 23]
1300-1200	C-O	Unsaturated esters		[22]
1160-1000	C-O, C=C, C-C-O (stretching)	Saturated esters, polysaccharides	Lignin, cellulose, Hemicelluloses	[23, 24]

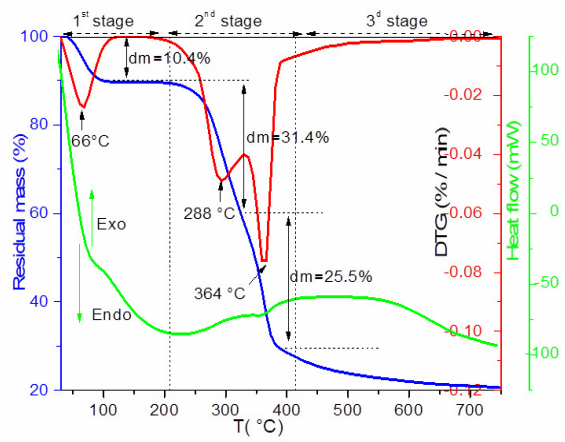

Figure 2: TGA-DTG-DSC of OS pyrolysis under N_2 atmosphere at a heating rate of 10°C/min

Thermogravimetric study

Thermal analysis is used to study and understand the pyrolysis process. Figure 2 shows the TGA and derivative thermogravimetric (DTG) curves of OS at a heating rate of 10 °C/min. According to this figure, the thermal degradation of OS follows the usual pattern for lignocellulosic materials, indicating three stages: moisture evaporation, main devolatilisation and continuous slight devolatilisation. The moisture evaporation

region occurred in the temperature range below 200 °C and corresponds to the first peak in the DTG profile. A mass loss of 10% was recorded, mainly attributed to the release of weakly bonded water molecules.

The main devolatilisation is located in the temperature range of 210-407 °C. This stage consists in a major mass loss (≈56%) ascribed to hemicellulose and cellulose degradation. Two distinct peaks are clearly observed on the DTG curves. The first peak was in the range of 210-342 °C, associated with a mass loss of 31%. The maximum rate of mass loss was recorded at 288 °C. Meanwhile, the second peak is located in the range of 342-407 °C, with a mass loss of 25.5%. As expected, the lower temperature shoulder appearing on the DTG curve represents the decomposition of hemicelluloses in OS and the higher temperature peak corresponds to the decomposition of the cellulose material.[26] However, chemical composition analysis (Table 2) shows that the hemicellulose content doesn't exceed 17% of OS mass. So, it could be deduced that the first peak is not attributed just to hemicellulose degradation. It is mentioned that cellulose is a high-molecular compound with long linear chain composed of D-glucosyl groups and a part of cellulose has crystalline structure, made of ordered micro-fibrils, which make its thermal degradation more difficult than that of hemicelluloses.[26,27] It should be noted that although these two stages are mainly characterized by the decomposition of cellulose and hemicelluloses,[28] simultaneous degradation of lignin is also present in that temperature interval, which is known to decompose slowly over a wide range of temperature. Over 407 °C, a slight devolatilisation indicated by the non-zero value of the DTG curve, could be due to the decomposition of lignin, which could continue up to 900 °C.[28]

The heat flow profile from DSC shows that the dehydration stage is endothermic, whereas the active pyrolysis and slow pyrolysis stage are exothermic.

Gas products analysis

The pyrolysis behavior of Tunisian OS by means of TGA–MS was not studied previously. TGA–MS measurements reproduce the evolution of the main gas products during the pyrolysis of biomass. This technique simultaneously determines the thermal decomposition and gas product distribution of a very small sample in real time. The utilization of MS techniques, along with thermal analysis, can facilitate a deeper insight into the kinetic scheme and, consequently, to understand the actual reaction mechanism. The present study was focused on the main volatile products of OS pyrolysis on the basis of both their relative intensities across the temperature range of 30-750 °C and on their relevancy. H_2, CH_4, H_2O, CO, C_2H_6 and CO_2 were assigned to the ion/mass intensities (m/z) 2, 16, 18, 28, 30 and 44 respectively.[29,30]

Figure 3 shows the MS spectra for raw OS as a function of temperature. Table 4 presents the major gas-phase and gas-solid reactions during the pyrolysis of OS. It could be clearly seen that most of the gas products were primarily generated in the same temperature range of 200-400 °C, except for H_2, which was produced at higher temperature (>550 °C). Then, accordingly to gas production, the overall temperature range measured by TG-MS could be divided into four stages, in contrast to the mass degradation profile. Firstly, the peaks at low temperatures (<200 °C) represented the drying process of the samples. Only H_2O and traces of methyl groups were observed in the spectra of the OS. Meanwhile, most of the authors that studied biomass pyrolysis have shown that there was no CH_4 release in this temperature range.[31] Consequently, the mass loss observed is related to the removal of unbound water.[29,31] In the second stage (200-400 °C), associated to the major mass loss, the main pyrolysis products detected were H_2O, CO, CO_2 and light hydrocarbons (CH_4 and C_2H_6). It is clear that the release of CO_2, CO and C_2H_6 was almost synchronous in the pyrolysis process, suggesting that these gases were produced by the same pyrolysis pathway. These facts revealed that decarboxylation (Eq. 19), decarbonylation (Eq. 20) and thermal cracking (Eq. 21) during biomass pyrolysis were simultaneous reactions, leading to the formation of CO_2, CO and C_2H_6, respectively. Regarding the fourth stage, two regions of gas release appeared: the first one corresponded to the production of CH_4, which was detected at temperatures ranging from 400 to 550 °C, with two peaks at 425 °C and 550 °C, respectively. In the pyrolysis of biomass, it is believed that most of the hydrocarbons, such as methane and ethylene, were produced from the thermal cracking of the tar (Eq. 22) formed during pyrolysis,[31] especially when an observed trace of H_2 existed in this temperature range. The second was related to H_2 evolution, which was observed,

respectively, in the decrease of CH_4 amount (above 550 °C); the product distribution observed in the last stage suggested that secondary reactions took place.

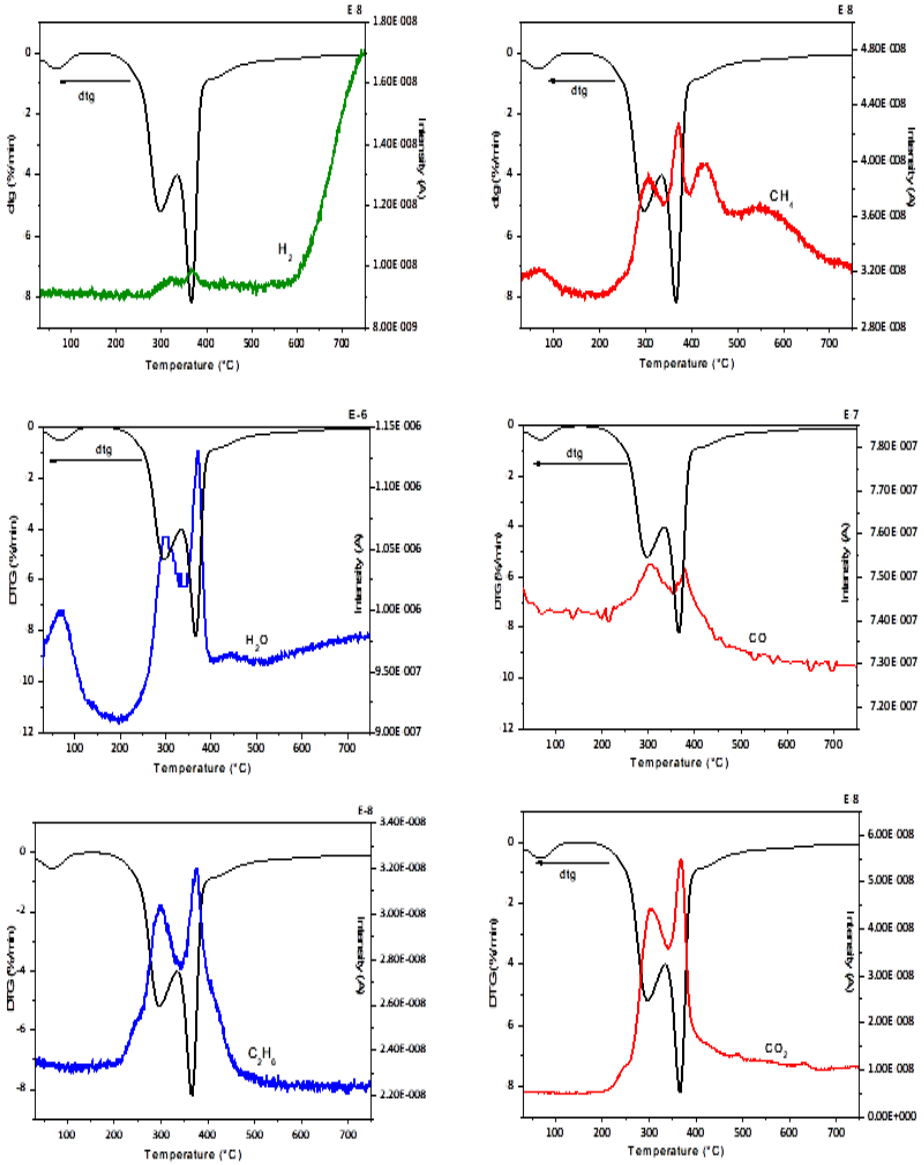

Figure 3: Evolution of gas products from OS pyrolysis at a heating rate of 10 °C/min

Table 4
Major gas-phase and gas-solid reactions during the pyrolysis of OS

Equation Nr.	Reaction	Equation
(19)	Decarboxylation	$R-COOH \rightarrow RH+CO_2$
(20)	Decarbonylation	$RCHO \rightarrow RH+CO$
(21)	Thermal cracking	$C_nH_m \rightarrow C_{n-x}H_{m-y}+H_2+CH_4+C$
(22)	Tar cracking	$C_nH_mO_p+(2n-p)H_2O \rightarrow nCO_2+(1/2m+2n-p)H_2$
(23)	Steam reforming of CH_4	$CH_4+H_2O \rightarrow CO+3H_2$
(24)	Thermal cracking CH_4	$CH_4 \rightarrow C+2H_2$

It has been shown that H_2 production is attributed to secondary reactions, such as tar cracking (Eq. 22) and/or steam reforming of methane (Eq. 23).[31,32] These reactions are brought by CO_2 and CO release. However, it is clear from the figure that any gas has been detected, except H_2. This fact reveals that H_2 is mainly generated by thermal cracking of methane (Eq. 24) during OS pyrolysis.

It can be concluded from MS analysis of OS pyrolysis that four stages of gaseous emissions were detected, as opposed to TGA analysis indicating only three stages of degradation. The evolution of CO_2, CO, C_2H_6 was synchronous, suggesting that these gases were produced by the same pyrolysis pathway.

Effect of heating rates

Figure 4 shows the thermal decomposition of OS under four heating rates (5, 10, 20 and 30 °C/min). Table 5 shows the maximum of mass-loss rate (R_{DTGmax}), the temperature corresponding to the maximum of mass-loss rate (T_{DTGmax}) and the reactivity (R_M) and char content at various heating rates at 750 °C. R_M is defined as the ratio between R_{DTGmax} and T_{DTGmax}, given as:

$$R_M = 100 \sum \frac{R_{DTG\,max}}{T_{DTG\,max}} \qquad (25)$$

The TGA curves for all the heating rates denote that the mass loss of OS mainly occurred at temperatures ranging from 200 °C to 460 °C. An obvious difference in the TG curves was found for the different heating rates. When the heating rate increased from 5 °C/min to 30 °C/min, the initial temperature of the main decomposition shifted to a higher temperature. The maximum mass loss rate increased and the peak temperature of the maximum rate shifted to higher temperatures with increasing heating rate. This behavior is observed in the literature for most lignocellulose biomasses.[5,11,33,34] In fact, an increase in the heating rate tends to delay the thermal degradation processes towards higher temperatures. This behavior could be attributed to heat transfer limitations with increasing heating rates.[33,35] Furthermore, at lower heating rates, heating of biomass particles occurs more gradually and leads to better heat transfer to the interior of the biomass.[34] On the other hand, it is clear from Table 5 that with an increasing heating rate from 5 to 30 °C/min, the maximum mass-loss rate increased from 0.126 wt%/min to 0.780 wt%/min, and that the peak temperature increased from 351 °C to 380 °C, indicating an increase in reactivity R_M (from 0.046 to 0.27%/min °C). This behavior is most probably due to a higher amount of thermal energy, which promotes the heat transfer between the surrounding medium to the interior of the biomass samples.[11] These results are similar to those determined by Damartzis *et al*.,[5] who found that the reactivity of wild cardoon leaves increases from 0.123 to 0.66% min^{-1} $°C^{-1}$ with an increasing heating rate from 5 to 30 °C/min.

By examining the effect of the heating rate on the solid residue, it can be seen that the residual solid mass does not change too much with the heating rate with respect to the initial mass. Indeed, a slight decrease in the amount of the residue is observed by increasing the heating rate from 5 to 30 °C/min with the exception of 20 °C/min, the residue value of which is high compared to the others. This result can be explained by the presence of reactions leading to the formation of char, independently of the heating rate. This result is in agreement with those reported in other papers in the literature.[5,36]

Kinetic analysis

Iso-conversional method for estimating activation energy

The model-free OFW and KAS methods were used to evaluate the apparent activation energy. The methods were employed at different heating rates ranging from 5 to 30 °C/min, for rate conversions varying from 0.20 to 0.80, to determine the variation of the apparent activation energy during the thermal decomposition process. Based on Equations (11) and (15), the plot of ln β and ln (ß/T^2) versus 1/T, respectively, should be a straight line. Apparent activation energy could be estimated from the slope of the line at various conversions α. Figure 5 (a, b) depicts the representative plots for the main stage of weight loss (*i.e*., stage II, 0.2<α<08). Because of low correlation, the values at conversion degrees below 0.2 and above 0.8 were not included.[5] The activation energies calculated using the OFW and KAS methods, as well as the correlation coefficients (R^2), are listed in Table 6. It can be seen that the determination coefficients are close to unit for all the lines, indicating well fitting results. The mean values of E_a obtained by the OFW and KAS methods were 228.20 and 232.55 kJ/mol, respectively. The results presented great

accordance, with a deviation below 2%. The small differences among the activation energy values could be caused by the difference in approximations used in these methods. Therefore, it can be concluded from Figure 5 and Table 6 that the model-free methods used are reliable in determining the activation energy.

Kinetic analysis results showed that activation energy is highly dependent on conversion. This result implies that OS pyrolysis is a complex process progressing through multi-step kinetics, which exhibits various apparent activation energies.[5] The variation of activation energy as a function of conversion degrees is shown in Figure 6.

For both methods, E_a increases sharply when rate conversion changes from 0.2 to 0.3. For the OFW model, E rises from 165 to 227 kJ/mol. It was assumed that the activation energy value in the conversion range 0.2-0.3 corresponded to the hemicelluloses degradation. As shown in the TG curves (Fig. 2), the maximum rate peak is reached at 288 °C, corresponding to a conversion rate of <0.3.

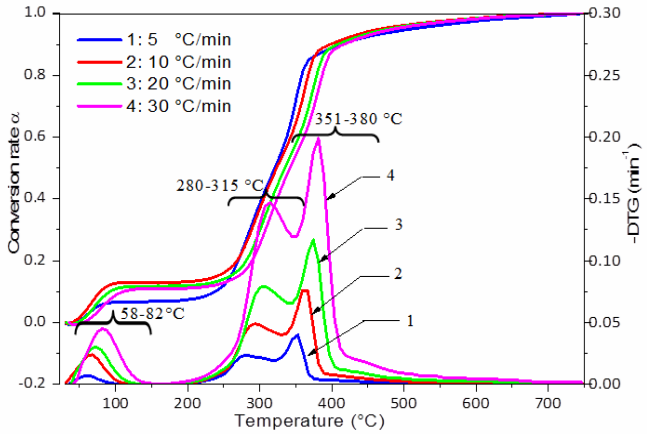

Figure 4: DTG curves of OS pyrolysis under N_2 atmosphere at various heating rates

Table 5
Characteristics of OS degradation at different heating rates

Heating rate β (°C/min)	Decomposition interval (°C)	$T_{shoulder}$ (°C)	$R_{shoulder}$ (%/min)	T_{peak} (°C)	R_{peak} (%/min)	R_M (%/min°C)	Solid residue (%, 750°C)
5	200-400	280	0.027	351	0.126	0.046	31.125
10	210-407	279	0.042	364	0.185	0.066	29.271
20	219-450	309	0.102	374	0.307	0.109	37.572
30	225-460	315	0.196	380	0.780	0.270	25.171

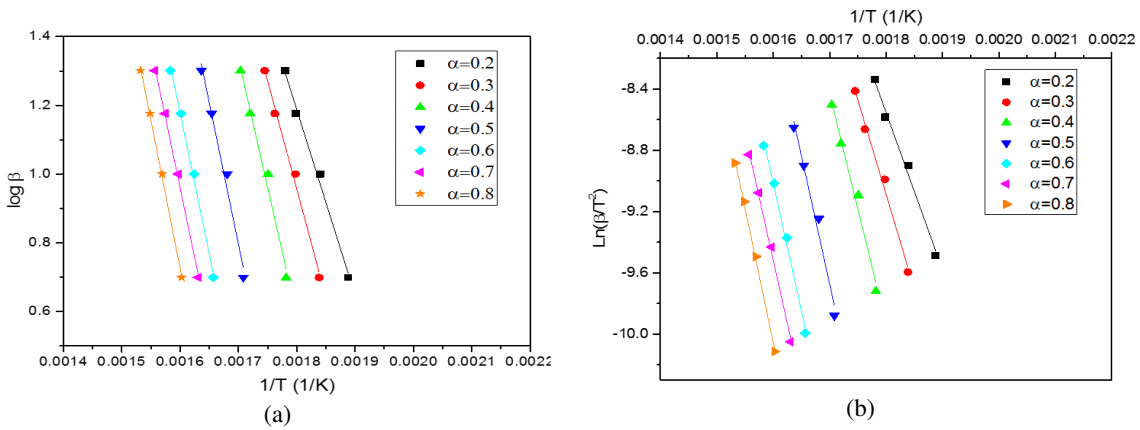

Figure 5: Estimation of activation energy using OFW (a) and KAS (b) methods for OS pyrolysis

Table 6
TGA pyrolysis of OS activation energies (E_a) and correlation factors (R^2) for different conversion values using OFW and KAS models

Conversion(x)	OFW model		KAS model	
	E_a(kJ/mol)	R^2	E_a(kJ/mol)	R^2
0.2	165.196	0.830	168.907	0.817
0.3	227.625	0.986	231.536	0.986
0.4	235.120	0.985	239.218	0.985
0.5	244.089	0.985	253.452	0.984
0.6	259.207	0.984	264.060	0.984
0.7	270.596	0.984	275.875	0.984
0.8	194.642	0.972	194.805	0.970
Average	228.199		232.550	

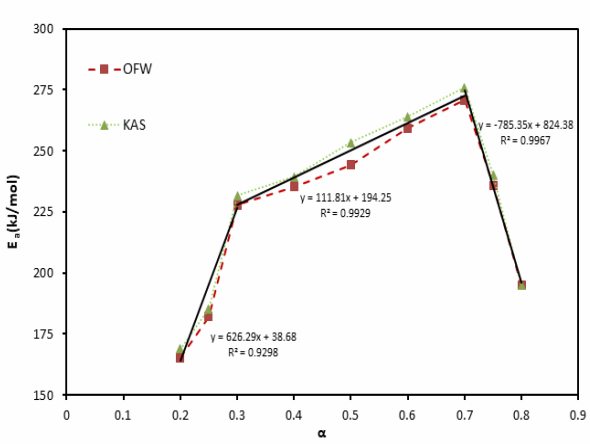

Figure 6: Activation energy distribution at different conversion rates determined by Friedman, OFW and KAS methods

The apparent activation energy increases were slightly similar for the conversion rate range between 0.3 and 0.7. It is well known (Fig. 2) that the main decomposition achieved below 70% conversion. The slight increase of the activation energy, E_a, values from 227 to 270 kJ/mol could be attributed to cellulose decomposition. Then, the activation energy decreased to 194.64 at the rate conversion value of 0.8, indicating the end of the main decomposition. Indeed, the activation energy presents the energy quantity necessary for the onset of chemical reaction. The same trend of activation energy evolution has been also seen by the KAS method. The average apparent activation energy for the olive stones was 229.2 and 232 kJ/mol by the OFW and KAS methods for conversion between 20% and 80%. Damartzis *et al*.[5] investigated the pyrolysis kinetics of cardoon and calculated E values of 224.1 kJ/mol for cardoon stems and 350.07 kJ/mol for cardoon leaves. The activation energy for the pyrolysis of pine wood ranged from 145 to 301 kJ/mol, depending on the conversion.[37] Lopez-Velazquez *et al*.[38] reported that the E_a values for the pyrolysis of orange waste varied between 120 and 250 kJ/mol. In general, the calculated E values for OS were similar to those reported in previous studies on biomass pyrolysis.

Because the average values of activation energy determined by the OFW and KAS methods were very close, we chose the average values of two (*i.e*., 230, 375 kJ/mol) as the value of activation energy used in the master-plots method.

Master-plots method for determining kinetic model

Using the predetermined value of activation energy E, along with the temperature measured as a function of α, P(u) can be calculated directly according to Equation (18). Then, the experimental master plots of $P(u)/P(u_{0.5})$ against α under various heating rates, can be plotted from the experimental data. Plotting $g(u)/g(0.5)$ against α corresponds to the theoretical master plots of various kinetic functions. Figure 7a shows the

theoretical master plots of g(α)/g(0.5) against α for different kinetic functions (Table 4). Figure 7b shows, in addition to the theoretical master plots of g(α)/g(0.5) against α for various kinetic models (Table 1), the experimental master plots of P(u)/P($u_{0.5}$) against α at heating rates β = 5, 10, 20 and 30 °C/min. It was found that the experimental master plots of different heating rates are practically identical, which may suggest that the kinetic degradation process could be described by single kinetics.[15,16] The comparison between the theoretical and the experimental results indicates that the current theoretical master plots could not match the experimental ones. However, the experimental master plots are close to the theoretical master plots O_2 and O_3. In order to determine whether the O_n model matches the experimental data, the plots of g(α)/g(0.5) against α at n = 4, 5 and 10, using O_n model, and P(u)/P($u_{0.5}$) against α according to the experimental data are presented in Figure 8. It is found that the experimental master plots lay between the theoretical master plots O_5 and O_{10}.

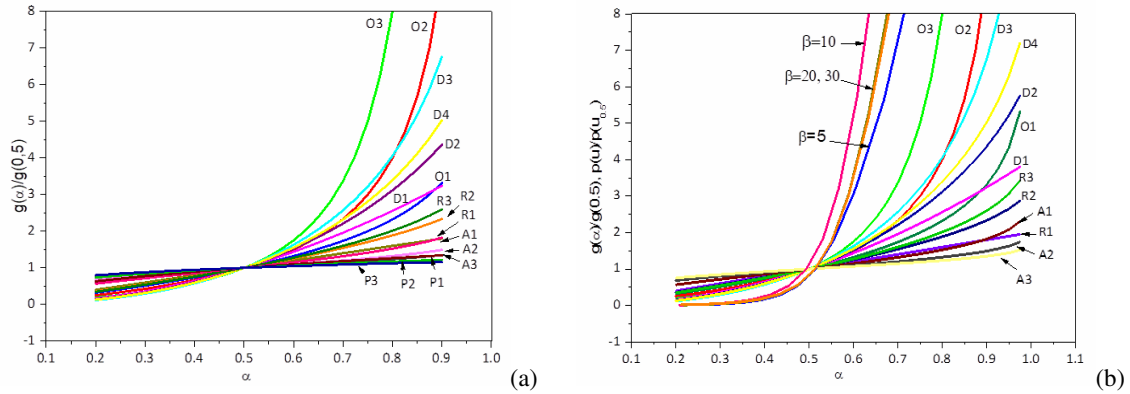

Figure 7: (a) Theoretical master plots of g(α)/g(0.5) against α for various reaction models (Table 4); (b) Theoretical master plots of g(α)/g(0.5) against α and experimental master plots of P(u)/P(u0.5) against α from experimental data obtained at heating rates of 5, 10, 20 and 30 °C/min

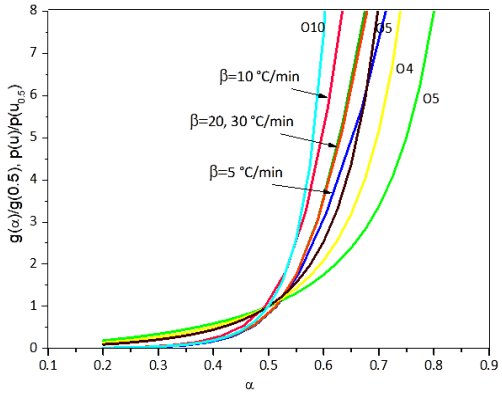

Figure 8: Theoretical O_n model of g(α)/g(0.5) against α and experimental master plots of p(u)/p($u_{0.5}$) against α at different heating rates

Table 7
Kinetic parameters calculated by the master-plot method

Sample	E (kJ/mol)	A (min^{-1})	n	R^2	Ref.
OS	230.375	5.6 x 10^{21}	6.2	0.9977	This study
D. tertiolecta	146.000	2.28 x 10^{13}	2.4	-	[20]
Cordgrass	183.5	4.29 x 10^{15}	3.34	-	[16]
C. vulgaris	418.6	6.18 x 10^{29}	9	0.9999	[15]

From the results, it can be assumed that order n (O_n) model, with an equation below Equation (19), describes the kinetic process for thermal decomposition of olive stones at various heating rates between 5 and 30 °C/min.

$$g(\alpha) = \frac{(1-\alpha)^{1-n} - 1}{1-n} \quad (26)$$

The accommodated O_n model with a non-integral exponent n was used for estimating the reaction order n and exponential factor A. The expression of O_n is introduced into Equation (8), and then Equation (26) turns into:

$$g(\alpha) = \frac{AE_a}{\beta R} P(u) = \frac{(1-\alpha)^{1-n} - 1}{1-n} \quad (27)$$

To obtain a relatively optimal value of n, it is investigated from 4 to 10 with the increment of 0.1 and a plot $[(1-\alpha)^{1-n}-1]/ (n -1)$ versus $E_aP(u)/\beta R$ by the linear least-square fitting procedure. The most preferable n is the value for which the intercept is closest to zero and R^2 is the highest. The highest R^2 at different βs, the most probable value of n and the corresponding A are listed in Table 7. The result showed that, for the pyrolysis of olive stones, the optimal n is 6.2, and the corresponding pre-exponential factor $A = 5.6.10^{21}$ min^{-1} with activation energy E_a of 230.375 kJ/mol. The most probable mechanism is the simple order reaction model function, $f(\alpha) = (1-\alpha)^{6.2}$.

A comparison of the obtained kinetic parameters of the pyrolysis of olive stones to those for other biomasses is shown in Table 7. The activation energy for the pyrolysis of olive stones is higher than that of smooth cordgrass,[16] and *D. tertiolecta*,[20] while lower than that of *Calluna vulgaris.*[15] An obvious difference was found in the reaction order and frequency factor for different biomasses by using the master-plots method. This difference could be explained by differences in the degradation mechanism of different biomasses.

CONCLUSION

The pyrolysis of olive stones was investigated by thermogravimetric analysis–mass spectrometry. According to gas evolution analysis, the thermal degradation of olive stones can be divided into four stages. Most of gas products (CO_2, light hydrocarbons and H_2O) were evolved in the second stage in the temperature range of 200-400 °C. Only H_2 was produced at higher temperatures (>550 °C). The initial temperature of pyrolysis and the temperature at which the pyrolysis rate reached the peak value shifted to the higher values with an increasing heating rate. The activation energy values estimated by OFW and KAS were 228.20 and 232.55 kJ/mol, respectively. The most probable reaction model function was $f(\alpha) = (1-\alpha)^{6.2}$ for thermal decomposition of olive stones by using the master-plots method. The frequency factor was estimated to be $A = 5.6 \times 10^{21}$ min^{-1}.

ACKNOWLEDGMENT: The authors would like to thank the Faculty of Chemical Engineering and Universiti Technologi MARA, for accepting the research internship of Mrs. Amina Bedoui.

REFERENCES

[1] I. Karaouzas, E. Cotou, T. Albanis, A. Kamarianos, N. Skoulikidis *et al*., *Environ. Toxicol*., **26**, 669 (2011), https://doi.org/10.1002/tox.20606

[2] K. R. Duarte, C. Justino, T. Panteleitchouk and A. Zrineh, A. C. Freitas *et al*., *Int. J. Environ. Sci. Technol*., **11**, 589 (2014), https://doi.org/10.1007/s13762-013-0268-2

[3] G. Várhegyi, J. A. Michael, E. Jakab and P. Szabó, *J. Anal. Appl. Pyrol*., **42**, 73 (1997), https://doi.org/10.1016/S0165-2370(96) 00971-0

[4] A. Chouchène, M. Jeguirim, B. Khiari, F. Zagrouba and G. Trouvé, *Resour. Conserv. Recyc*., **54**, 271 (2010), https://doi.org/10.1016/j.resconrec.2009.04.010

[5] Th. Damartzis, D. Vamvuka, S. Sfakiotakis and A. Zabaniotou, *Bioresour. Technol*., **102**, 6230 (2011), https://doi.org/10.1016/j.biortech.2011.02.060

[6] J. Guo and A. C. Lua, *Biomass Bioenerg*., **20**, 223 (2001), https://doi.org/10.1016/S0961-9534(00)00080-5

[7] A. Agrawal and S. Chakraborty, *Bioresour. Technol*., **128**, 72 (2013), https://doi.org/10.1016/j.biortech.2012.10.043

[8] A. Ounas, A. Aboulkas, K. El Harfi, A. Bacaoui and A. Yaacoubi, *Bioresour. Technol*., **102**, 11234 (2011), https://doi.org/10.1016/j.biortech.2011.09.010

[9] A. T. Hoang, H. C. Ong, I. M. R. Fattah, C. T. Chong, C. K. Cheng *et al*., *Fuel Process. Technol*., **223**, 106997 (2021), https://doi.org/10.1016/j.fuproc.2021.106997

[10] O. A. Akinwale, F. G. Johann, M. Carrier, L. M. Edson and J. H. Knoetze, *Fuel Process. Technol*., **106**, 310 (2013), https://doi.org/10.1016/j.fuproc.2012.08.014

[11] S.-S. Kim, A. Shenoy and F. A. Agblevor, *Bioresour. Technol*., **156**, 297 (2014), https://doi.org/10.1016/j.biortech.2014.01.066

[12] J. A. Caballero, J. A. Conesa, R. Font and A. Marcilla, *J. Anal. Appl. Pyrol.*, **42**, 159 (1997), https://doi.org/10.1016/S0165-2370(97)00015-6
[13] M. C. Blanco López, C. G. Blanco, A. Martínez-Alonso and J. M. D. Tasco, *J. Anal. Appl. Pyrol.*, **65**, 313 (2002), https://doi.org/10.1016/S0165-2370(02)00008-6
[14] U. Özveren and Z. S. Özdoğan, *Biomass Bioenerg.*, **58**, 168 (2013), https://doi.org/10.1016/j.biombioe.2013.08.011
[15] C. Chen, X. Ma and Y. He, *Bioresour. Technol.*, **117**, 264 (2012), https://doi.org/10.1016/j.biortech.2012.04.077
[16] L. Wilson, W. Yang, W. Blasiak, G. R. John and C. F. Mhilu, *Energ. Convers. Manag.*, **52**, 191 (2011), https://doi.org/10.1016/j.enconman.2010.06.058
[17] C. D. Doyle, *J. Appl. Polym. Sci.*, **24**, 639 (1962), https://doi.org/10.1002/app.1962.070062406
[18] H. E. Kissinger, *Anal. Chem.*, **29**, 1702 (1957), https://doi.org/10.1021/ac60131a045
[19] T. Ozawa, *B. Chem. Soc. Jpn.*, **38**, 1881 (1965), https://doi.org/10.1246/bcsj.38.1881
[20] S. Zou, Y. Wu, M. Yang, C. Li and J. Tong, *Bioresour. Technol.*, **101**, 359 (2010), https://doi.org/10.1016/j.biortech.2009.08.020
[21] R. Baccar, J. Bouzid, M. Feki and A. Montiel, *J. Hazard. Mater.*, **162**, 1522 (2009), https://doi.org/10.1016/j.jhazmat.2008.06.041
[22] C. J. Durán-Valle, M. Gómez-Corzo, J. Pastor-Villegas and V. Gómez-Serrano, *J. Anal. Appl. Pyrol.*, **73**, 59 (2005), https://doi.org/10.1016/j.jaap.2004.10.004
[23] F. Xu, J. Yu, T. Tesso, F. Dowell and D. Wang, *Appl. Energ.*, **104**, 801 (2013), https://doi.org/10.1016/j.apenergy.2012.12.019
[24] M. Asadieraghi and W. M. A. Wan Daud, *J. Anal. Appl. Pyrol.*, **115**, 379 (2015), https://doi.org/10.1016/j.jaap.2015.08.017
[25] M. Jagtoyen and F. Derbyshire, *Carbon*, **36**, 1085 (1998), https://doi.org/10.1016/S0008-6223(98)00082-7
[26] J. F. González, S. Roman, J. M. Encínar and G. Martínez, *J. Anal. Appl. Pyrol.*, **85**, 134 (2009), https://doi.org/10.1016/j.jaap.2008.11.035
[27] Z. Ma, D. Chen, J. Gu, B. Bao and Q. Zhang, *Energ. Convers. Manag.*, **89**, 251 (2015), https://doi.org/10.1016/j.enconman.2014.09.074
[28] S. S. Idris, N. Abd Rahman, K. Ismail, A. B. Alias, Z. Abd Rashid *et al.*, *Bioresour. Technol.*, **101**, 4584 (2010), https://doi.org/10.1016/j.biortech.2010.01.059
[29] L. Sanchez-Silva, D. López-González, J. Villaseñor, P. Sánchez and J. L. Valverde, *Bioresour. Technol.*, **109**, 163 (2012), https://doi.org/10.1016/j.biortech.2012.01.001
[30] S. Wang, H. Lin, B. Ru, G. Dai, X. Wang *et al.*, *Fuel*, **185**, 763 (2016), https://doi.org/10.1016/j.fuel.2016.08.037
[31] Y. F. Huang, W. H. Kuan, P. T. Chiueh and S. L. Lo, *Bioresour. Technol.*, **102**, 3527 (2011), https://doi.org/10.1016/j.biortech.2010.11.049
[32] M. Widyawati, T. L. Church, N. H. Florin and A. T. Harris, *Int. J. Hyd. Energ.*, **36**, 4800 (2011), https://doi.org/10.1016/j.ijhydene.2010.11.103
[33] S. S. Idris, N. Abd Rahman and K. Ismail, *Bioresour. Technol.*, **123**, 581 (2012), https://doi.org/10.1016/j.biortech.2012.07.065
[34] S. Ceylan and Y. Topçu, *Bioresour. Technol.*, **156**, 182 (2014), https://doi.org/10.1016/j.biortech.2014.01.040
[35] D. Vamvuka, E. Kakaras, E. Kastanaki and P. Grammelis, *Fuel*, **82**, 1949 (2003), https://doi.org/10.1016/S0016-2361(03)00153-4
[36] T. Fateh, T. Rogaume, J. Luche, F. Richard and F. Jabouille, *Fire Saf. J.*, **58**, 25 (2013), https://doi.org/10.1016/j.firesaf.2013.01.019
[37] S. Kim, J. Kim, Y.-H. Park and Y.-K. Park, *Bioresour. Technol.*, **101**, 9797 (2010), https://doi.org/10.1016/j.biortech.2010.07.094
[38] M. A. Lopez-Velazquez, V. Santes, J. Balmaseda and E. Torres-Garcia, *J. Anal. Appl. Pyrol.*, **99**, 170 (2013), https://doi.org/10.1016/j.jaap.2012.09.016